Eu³⁺   Tb³⁺

Showcasing research from Professor Li Wang's laboratory, School of Chemistry, Capital Normal University, Beijing, China.

A step forward in unraveling the lanthanide discrimination puzzle: structure–selectivity relationship based on phenanthroline diimide ligands towards europium and terbium detection in water

Two isomeric phenanthroline diimides were found to be capable of selectively sensing europium(III) and terbium(III) in aqueous solutions, which could contribute to a fundamental understanding of selective photoluminescence sensing of rare earth elements (REEs) and represents the first investigation into Eu(III)/Tb(III) sensing and discrimination in water.

As featured in:

See Xiaoyan Tang, Li Wang *et al.*, *J. Mater. Chem. C*, 2024, **12**, 6056.

Check for updates

A step forward in unraveling the lanthanide discrimination puzzle: structure–selectivity relationship based on phenanthroline diimide ligands towards europium and terbium detection in water†

Yu Kang,‡[ab] Haoyu Li,‡[a] Mingjie Bao,‡[a] Yuan Zheng,[a] Ludi Wang, [a] Dezhu Liu,[a] Jiahui Li,[a] Ziyi Wei,[a] Chaoqun Weng,[b] Guo Wang,[a] Xiaoyan Tang*[b] and Li Wang *[a]

The substantial expansion of technology and geopolitical needs necessitate the search for innovation and alternatives in the supply and recycling of lanthanides. As a prerequisite, lanthanide sensing proves invaluable for identifying lanthanides and locating high-value streams before resorting to laborious extraction processes. Equally important, this selective sensing can potentially contribute to environmental management and optimization of extraction processes. Presently, there are no systematic guidelines for designing highly selective sensing and extraction ligands. In this contribution, we present the successful demonstration of two isomeric phenanthroline diimides capable of selectively sensing europium(III) and terbium(III) in aqueous solutions. The limits of detection (LOD) for both cations were measured to be 15 nM and 2.95 μM, respectively, with superior anti-inference properties with other lanthanides. Data fitting from ratiometric titrations revealed distinct solution coordination species evolutions even though coordination sites were identical for the two isomerides. Close examination of photophysical and electrochemical characteristics, together with DFT calculations, revealed that subtle structural modifications influenced ligand solubilities (intermolecular interaction), the nature of emission states, and molecular energy levels. These ligand structural modifications ultimately led to selective sensing of Eu(III) and Tb(III) in aqueous media. We believe that this work contributes to a fundamental understanding of the selective photoluminescent sensing of rare earth elements (REEs) and represents the first investigation into Eu(III)/Tb(III) sensing and discrimination in water.

Introduction

Rare earth elements (REEs, referring to all lanthanides together with scandium and yttrium) are important strategic elements and play irreplaceable roles in a wide range of applications, from lighting,[1–3] sensing[4,5] and catalysis[6,7] to supramolecular construction,[8,9] green energy generation,[10,11] biosensing and biomedicine[4,12–14] Since the production of individual lanthanides require tedious industrial processes by leveraging mainly subtle radii differences among the lanthanide series, it is highly labour-intense and imposes enormous environmental burdens.[15–17] Moreover, exponential spikes in the production and consumption of REEs result in the unexpected enhancement of these elements in the environment and biosystems, which eventually ends up back in mankind through bioaccumulation and food chain transfers, causing neurotoxicity and detrimental to the lungs, liver and other organs.[18,19] Therefore, rapid REE screening techniques are of utmost importance.[20,21]

The currently used technologies for quantitative determination of individual REEs are mostly instrument-based, including mass spectroscopy-based techniques such as inductively coupled plasma mass spectrometry (ICP-MS) and its related forms [ICP-TOF (time-of-flight)-MS, HR (high resolution)-ICP-MS and MC (multi-collector)-ICP-MS], as well as emission-

[a] Department of Chemistry, Capital Normal University, Haidian District, Beijing, 100048, China. E-mail: liwang862011@gmail.com

[b] Beijing National Laboratory for Molecular Sciences, Key Laboratory of Polymer Chemistry and Physics of Ministry of Education, Centre for Soft Matter Science and Engineering, College of Chemistry and Molecular Engineering, Peking University, Haidian District, Beijing, 100871, China. E-mail: xiaoyan.tang@pku.edu.cn

† Electronic supplementary information (ESI) available. See DOI: https://doi.org/10.1039/d4tc00197d

‡ Yu Kang, Haoyu Li and Mingjie Bao contributed equally to this work.
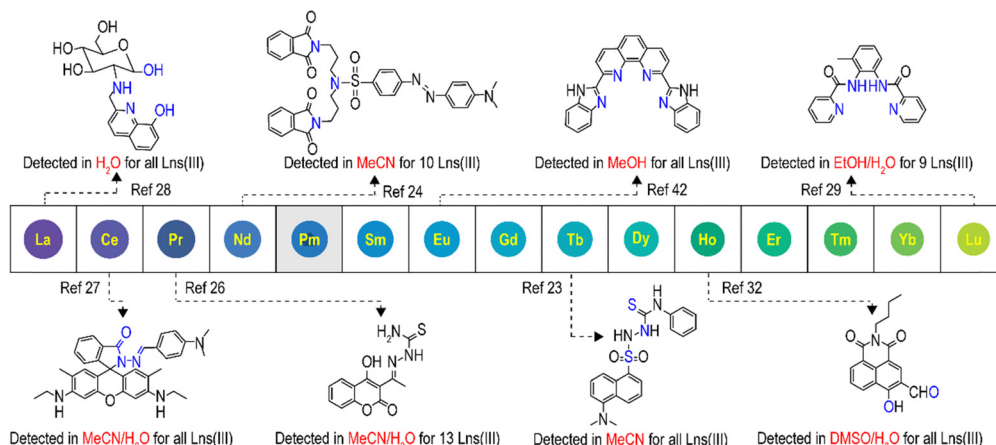
Scheme 1 Representative small molecules used for Lns(III) detection. The coordination sites were marked in blue for each structure (no reported binding modes for Pr(III)). The sensing conditions are emphasized in red.

based techniques like ICP-OES (optical emission spectrometry), INAA (instrumental neutron activation analysis), XRF (X-ray fluorescence spectrometry), LIBS (laser-induced breakdown spectroscopy) and MP-AES (microwave plasma atomic emission spectrometry).[19,20] These technologies feature high sensitivity, anti-interference, multi-element capability, ease of operation and high accuracy. However, drawbacks such as high cost, tedious sample preparation, rigorous instrument operation requirements and non-portability hinder on-site application and substantially lengthen the sample processing time. Luminescence sensors, in comparison, are promising alternatives, for which the rational ligand/chelator design is the determinant.[2,20,21]

In general, steady-state luminescence-based detection of REEs can be divided into two main categories: the probe-centered and REE-centered processes.[20] For the former, the interaction of the probe with REEs alters the emission of the probe itself, causing either enhanced, reduced or ratiometric change in emission intensities. In the latter case, REE-originated emissions are detected from the Laporte forbidden

f–f transition through a process dubbed sensitization, which can happen *via* through-space energy transfer (Förster resonance energy transfer), through-bond electron exchange (Dexter energy transfer) or photoinduced, redox-mediated pathways.[20,22] Most reported sensors are based on the first two mechanisms; Eu(III) and Tb(III) turned out to be more easily sensitized because of the wider band gaps of the two cations among all REEs, which eliminates emission-quenching possibilities *via* non-radiative energy losses.[2,20] Thus, a lot of works have been published in the literature for Eu(III) and Tb(III) detection, while only a small portion has been done in aqueous media (this also holds true for other REEs, Scheme 1),[23–42] despite most real-world detections being done in water.[20,28,37,38,43] It is generally believed that selective REE detection in aqueous media with high sensitivity is tricky, mainly for following reasons: (1) synthetic and purification obstacles for water-soluble ligands themselves with respect to lipophilic ones;[44,45] (2) water could quench the emission for the ligand and complex because of its high polarity (rich in high energy vibrational O–H stretches and its overtones) and more polarized ligand/complex excited state (compared to the ground state), especially for near-infrared emissions;[4,20] (3) the strong coordination ability of water molecules requires more desolvation energy for a stronger ligand to give stable complexes,[8] while somewhat reducing the ligand selectivity. Furthermore, organic ligand-based REE photoluminescence sensors are highly pursued for their defined molecular structures, readily adjustable emissions, ease of preparation and repeatable production.[20,21,46] Our research studies are thus focusing on the rational design of organic ligands for the selective sensing of individual REEs in aqueous media and trying to uncover the structure function relationship to guide future ligand design.

In this work, we demonstrate, to the best of our knowledge, the very first work on selective sensing of Eu(III) and Tb(III) in aqueous solution with the interference of all other lanthanide(III) cations. Two structural isomers were designed and synthesized based on phenanthroline diimide architecture according to our recent works. We show that reducing the number of alkyl chains on well-studied phenanthroline

Li Wang earned his BSc degree from Wuhan University in 2009 and received his PhD from Changchun Institute of Applied Chemistry in 2015 under the supervision of Professor Y. Geng. After graduation, he conducted his 5-year postdoctoral research at North Dakota State University, Houston Methodist Research Institute and Colorado State University before securing a research professor position at the Institute of Process Engineering, CAS, in 2020. In 2021, he moved to Capital Normal University to embark on his independent career focusing on the coordination and separation of f-block elements.

Li Wang

diamide ligands could reduce energy barriers for the coordination of ligands towards lanthanide and actinide cations, while still keeping tetradentate ONNO binding pockets.[47–49] Besides, by dedicated selection of solubilizing end groups, the coordination modes of final complexes could be fine-tuned, leading to superior extraction selectivity towards Lns(III)/Ans(III) and Lns(III)/Lns(III).[50] With the aim of further shrinking coordination pockets to adjust the coordination and selectivity, we have moved the carbonyl group one carbon away from the phenanthroline framework, giving **Phen-2DIBA-re**. To our surprise, **Phen-2DIBA-re** displayed totally different coordination selectivity in comparison with the pristine **Phen-2DIBA**. Mechanism analyses showed distinctly different species evolution for the two isomerides despite having the same coordination environment. DFT calculations, together with close photophysical analyses, indicated the excited states of **Phen-2DIBA** to be π–π in nature, while it is mixed π–π with intra-ligand charge transfer (ILCT) for **Phen-2DIBA-re**. Although **Phen-2DIBA-re** showed reduced binding affinity towards all Lns(III) with respect to **Phen-2DIBA**, more favourable energy levels in the former facilitated the sensitization of smaller Tb(III) in comparison with the selective sensing of Eu(III) for **Phen-2DIBA** in water. This work represents a detailed approach towards selective lanthanide binding and sensitization through ligand structure modification, which thus could help to establish the structure–function relationship for intragroup lanthanide discrimination and extraction.

Results and discussion

Ligand design and characterizations

To prove the aforementioned hypothesis, carbonyl groups were moved one carbon away from the phenanthroline core to give the analogue of **Phen-2DIBA** (designated as **Phen-2DIBA-re**; imides were reversed from the phenanthroline side, as marked in blue in Fig. 1). **Phen-2DIBA** and **Phen-2DIBA-re** bore ONNO binding architecture but with different binding pocket sizes. The phenyl-substituted derivatives of **Phen-2DIBA-re** were first reported by Shinsaku with the purpose to explore new ONNO ligands to replace salen ligands for copper complexation.[51] Different from the preparation of **Phen-2DIBA**, **Phen-2DIBA-re** was synthesized by the reaction of 1,10-phenanthroline-2,9-diamine with glutaric anhydride in DMF, yielding the ligand with high purity after precipitation by adding water to the reaction mixture. The chemical identity of the final ligand was confirmed by NMR (^{1}H, ^{13}C and 2D H–H COSY) and HRMS (Fig. S1–S4 and Table S1, ESI†). Despite the small structural changes of the two ligands, the solubility varied a lot. As given in Fig. S5 (ESI†), **Phen-2DIBA** (5 mM) could dissolve in 1.5 M HNO$_3$, which was previously assigned to contributions from the protonation of phenanthroline and carboxyl groups.[47] Meanwhile, for the close structural analogue, **Phen-2DIBA-re** gave suspensions even after heating at 80 °C for 10 minutes, which further emphasized the contribution of ligand arrangement to the overall solubility. Furthermore, the two ligands displayed distinct photophysical behaviours. As given in Fig. 1b, **Phen-2DIBA** features well-defined absorption and emission peaks, which are typical characteristics originating from the stiff ligand architecture.[42,47,48,52] All three subpeaks from **Phen-2DIBA** were ligand-originated, as evidenced by excitation spectra monitored at corresponding emissions (Fig. S6a, ESI†). The water solution of **Phen-2DIBA** displayed weak blue emission with the relative photoluminescence quantum yield of 0.036 (Fig. S7 and Table S2, ESI†). DFT calculations showed that the emission states were mainly contributed by HOMO−2 to LUMO, with typical ligand-centred π–π transitions (Fig. 1c).
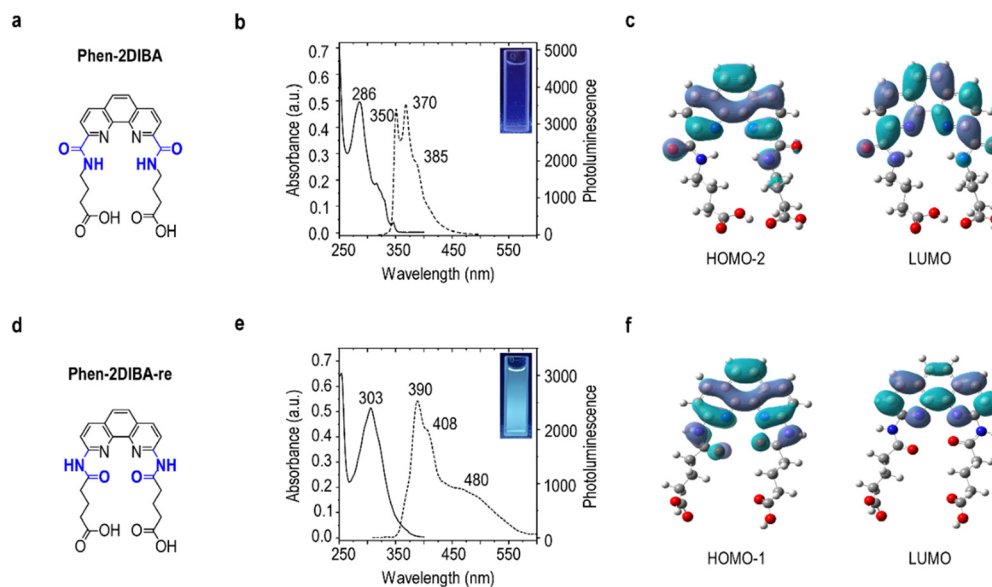

Fig. 1 Ligand photophysics. Molecular structures, absorption/emission spectra (excited at 300 nm) and molecular orbital (MOs) distributions for the main emissive species of (a)–(c) **Phen-2DIBA** and (d)–(f) **Phen-2DIBA-re**. The structural differences are marked in blue in (a) and (d). The inset images in (b) and (e) show the emission of **Phen-2DIBA** and **Phen-2DIBA-re** in water with concentrations of 2×10^{-5} M under the excitation of 365 nm LED.

6058 | *J. Mater. Chem. C*, 2024, **12**, 6056–6063

This journal is © The Royal Society of Chemistry 2024

In comparison, **Phen-2DIBA-re**, with its reverse imide bonds, displayed totally different absorption and emission (Fig. 1e), both of which are red-shifted compared with **Phen-2DIBA**. Moreover, broader and smoother peaks were detected for **Phen-2DIBA-re**, indicating the involvement of charge transfer state, which was further validated by DFT calculations (Fig. 1f). The greater spatial separation of the carbonyl groups from the phenanthroline core due to imine groups disrupted the extension of π-systems, allowing the electron redistribution from the carbonyl groups in the HOMO-1 ground state to electron-deficient phenanthroline-centred LUMO orbitals (Fig. 1f). We also noted that a broad emission peak from 450 nm to 550 nm existed for **Phen-2DIBA-re**. The excitation spectra indicated this peak was from the ligand, the same with the emissions located at 390 and 408 nm (Fig. S6b, ESI†). Further temperature-dependent absorption and emission of **Phen-2DIBA-re** under same conditions confirmed that the broad peak could be originated from the aggregation of **Phen-2DIBA-re** (Fig. S8, ESI†). The water solution of **Phen-2DIBA-re** was bluish green with the emission quantum yield of 0.043, slightly higher than that of **Phen-2DIBA**. In a nutshell, structural modification by reversing imide groups resulted in obvious changes in photophysical properties, as evidenced experimentally and theoretically.

Intragroup lanthanide discrimination

To further elucidate the effect of ligand structure changes on lanthanide-sensing properties, the spectral changes of **Phen-2DIBA** and **Phen-2DIBA-re** towards all Lns(III) (in nitrate salt forms) were examined. As shown in Fig. 2a, adding Lns(III) (10 equivalents of the ligand) into the aqueous solution of **Phen-2DIBA** resulted in redshifts and more intense absorption peaks, which strongly indicated the existence of metal–ligand interactions for **Phen-2DIBA** towards all Lns(III).[53] At the same time, almost totally quenched ligand emission was observed from Pr(III) to Yb(III), and selective strong sensitization of Eu(III) in water was detected, which allowed the specific identification of Eu(III) among all other Lns(III) (Fig. 2c and inset photos, Fig. S9, ESI†). The sensitization was further confirmed by the excitation spectra monitored at the characteristic Eu(III) emission peaks at 591 and 614 nm ($^5D_0$ to $^7F_1$ and $^7F_2$),[54] which solidly confirmed that the strong Eu(III) emissions were from the excitation of **Phen-2DIBA**. It should be pointed out that **Phen-2DIBA** did also respond to Sm(III) and Tb(III), resulting in the sensitization of both cations except Eu(III), but to a much weaker extent (Fig. 2b and Fig. S9 and S10, ESI†). Unexpectedly, the structural isomer **Phen-2DIBA-re** behaved distinctly towards Lns(III) in water with respect to **Phen-2DIBA**. No obvious absorption peak changes were detected with the addition of excess metal cations to the ligand solution in water for **Phen-2DIBA-re**, which are believed to be indicators for weaker metal–ligand interactions (smaller binding constants). Thus, although binding atoms were largely the same for both the isomerides (being ONNO tetradentate as demonstrated in the following section), more separated ON distances (through-bond distance) weakened the metal binding. Similarly, weaker quenching effects were observed in the emission spectra (Fig. 2e and f).
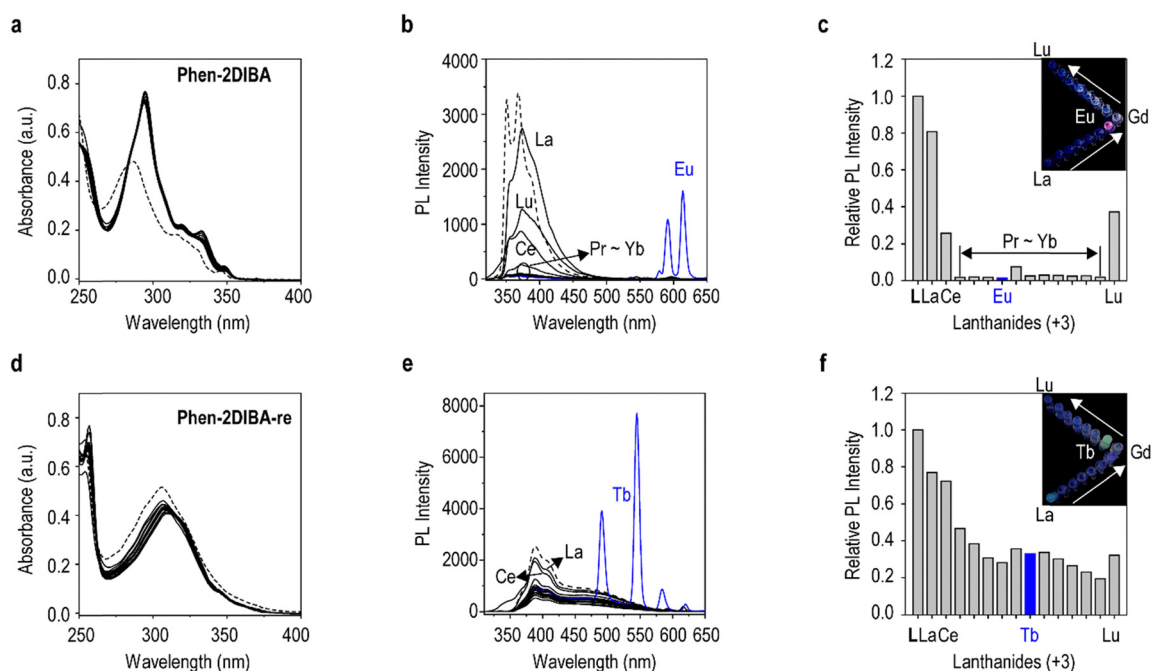
Fig. 2 Intragroup lanthanide discrimination. Absorption, emission and relative PL intensities for (a)−(c) **Phen-2DIBA** and (d)−(f) **Phen-2DIBA-re** in water. Conditions: ligand concentration of 2×10^{-5} M with 10 equivalents of Ln(III) except Pm(III); all measurements were done in DI water. Absorption and emission from the two ligands are given in dashed lines, and the selective sensing of Eu(III) and Tb(III) is marked in blue. Relative PL intensity in panels (c) and (f) refer to the ratio of PL intensity from the maximum ligand-orientated region (in the range of 350 to 500 nm) for each lanthanide to the initial PL maximum of the ligand. The inset images in panels (c) and (f) show the photos of lanthanide selectivity under 365-nm excitation.

This journal is © The Royal Society of Chemistry 2024

J. Mater. Chem. C, 2024, **12**, 6056–6063 | **6059**

Despite the overall weak interactions of **Phen-2DIBA-re** towards all Lns(III), the sensitization for Tb(III) was ultra-efficient (Fig. 2e and Fig. S11, S12, ESI†). Characteristic Tb(III)-originated transitions from $^5D_4$ to ^7F_J (J = 3, 4, 5, and 6) were observed immediately after the addition of Tb(III) into the aqueous solution of **Phen-2DIBA-re**, giving distinctive bright-green emissions (inset photos in Fig. 2f). The sensitization process was verified by monitoring excitations at the first two intense Tb(III) emission peaks of 491 and 545 nm, which resembled the absorption of **Phen-2DIBA-re**, demonstrating the origin of Tb(III) emissions. Furthermore, **Phen-2DIBA** and **Phen-2DIBA-re** responded to Eu(III) and Tb(III) very quickly, within 20 seconds (the minimum time requested in our case to thoroughly mix the ligand and metal cations), as shown in Fig. S13 (ESI†). In fact, Eu(III) and Tb(III) are among the rarest and most valuable REEs and ranked as the most economically critical REEs by the United States and Canada for their ease of sensitization to give highly emissive complexes.[20,37,41] Thus, a lot of work has been published in the literature for Eu(III) and Tb(III) detection, while only a small portion is done in aqueous media.[20,21,37,38,40,41,55,56] Besides, to the best of our knowledge, fewer studies have been conducted to show the selective sensitization of Eu(III) and/or Tb(III) towards all other Lns(III), and no work has been done to unravel the ligand structure origination of the selectivity; thus, our work represents the first of this kind.

The anti-interference performance is an important criteria for Lns(III) sensors. Thus, the preferable selectivity of **Phen-2DIBA** towards Eu(III) and **Phen-2DIBA-re** to Tb(III) were further

investigated by adding competitive Lns(III) into **Phen-2DIBA/Eu(III)** and **Phen-2DIBA-re/Tb(III)** solutions, and the emission changes were monitored at the highest characteristic Eu(III)/Tb(III) emissions. As depicted in Fig. S14 and S15 (ESI†), the addition of second Lns(III) cations into either **Phen-2DIBA/Eu(III)** or **Phen-2DIBA-re/Tb(III)** solutions only reduced the intensities of Eu(III)-/Tb(III)-originated emissions, implying the superior selectivity of both the ligands. Similar results were observed when **Phen-2DIBA** and **Phen-2DIBA-re** were added into the mixtures of Eu(III) and Tb(III) with other Lns(III) (Fig. S14 and S15, ESI†). Furthermore, for real-world applications, the sensing and/or extraction of Lns(III) are typically done in acid (for example, in Lns(III) recycling from acid mine drainage (AMD) and electronic waste); thus, the selective sensing performance of Lns(III) for **Phen-2DIBA** and **Phen-2DIBA-re** was further demonstrated in HNO_3 with pH of 3 (acidity for AMD).[20,37] Fig. S16 (ESI†) showed that the selectivity of **Phen-2DIBA** towards Eu(III) persisted in dilute HNO_3, while no obvious differences for **Phen-2DIBA-re** with all Lns(III) were observed. The sensitization stability of **Phen-2DIBA** and **Phen-2DIBA-re** towards Eu(III) and Tb(III) was further demonstrated in the pH range of 1–7, and the sensitization of **Phen-2DIBA** towards Eu(III) was stable under all pH levels for at least 10 hours, while **Phen-2DIBA-re** was found capable of sensitizing Tb(III) at pH above 5 (Fig. S17, ESI†). These observations emphasized the importance of the ligand structure on the overall Lns(III) sensing. Finally, the successful detection of both ligands towards Eu(III) and Tb(III) in real-world cases was illustrated in stimulated industrial waste streams (Fig. S18, ESI†).
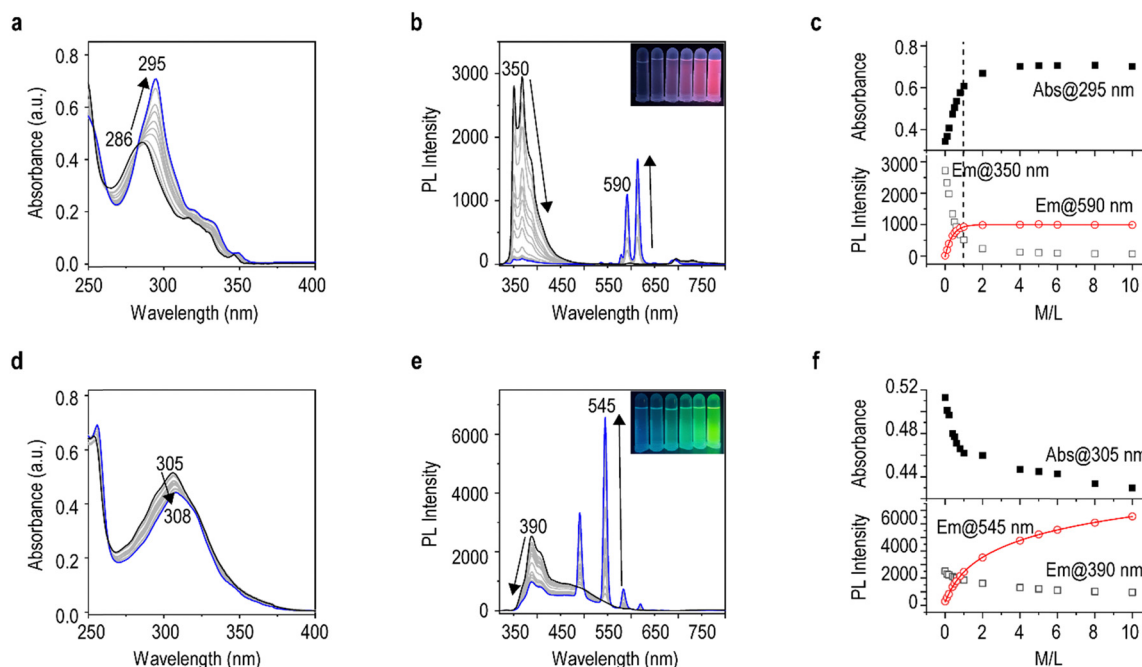

Fig. 3 Ratiometric detection analyses. (a) and (d) Absorption and (b) and (e) emission spectra changes with the addition of Eu(III)/Tb(III) into 2×10^{-5} M **Phen-2DIBA/Phen-2DIBA-re** in water. The evolutions of absorption (up) and emission (bottom) at characteristic wavelengths as functions of M/L ratios for (c) **Phen-2DIBA** and (f) **Phen-2DIBA-re**. The red curves show the nonlinear fitting to the data (ExpGro 1 in panel (c) and ExpGro 3 in panel (f)). The arrows in all figures are used to show changes during the titrations.

6060 | *J. Mater. Chem. C*, 2024, **12**, 6056–6063

This journal is © The Royal Society of Chemistry 2024

Spectra titrations and solution coordination analyses

To better understand the selective sensing performance of **Phen-2DIBA** and **Phen-2DIBA-re** towards Eu(III) and Tb(III) in aqueous media, absorption and emission spectra, as functions of metal-to-ligand ratios, were evaluated. For **Phen-2DIBA**, the gradual addition of Eu(III) cations into the 2×10^{-5} M water solution of **Phen-2DIBA** resulted in a stepwise increase of absorbances, accompanied by a red-shifted absorption maximum from 286 nm to 295 nm (M/L from 0 to 10, Fig. 3a). At the same time, photoluminescence of same solutions, monitored side-by-side with absorption titrations, gave ratiometric changes of ligand emissions together with Eu(III)-originated emissions. With the M/L ratio of 10, the ligand emission was almost totally quenched to give intense Eu(III) emission in water, which could be clearly detected with the naked eye under 365-nm excitation (Fig. 3b, inset). The absorption/emission intensities were then plotted as functions of M/L ratios, and in all cases, the data best fitted with a single exponential decay/growth function, indicating predominant evolution of one species.[57] The mole-ratio method further revealed that this major species had an M/L ratio of 1, consistent with our recent report, with the stable species verified by single-crystal X-ray diffraction.[47] Meanwhile, for **Phen-2DIBA-re**, the addition of Tb(III) only caused weakened absorption, with a small bathochromic shift from 305 to 308 nm. Nevertheless, strong sensitization processes were detected, with intense Tb(III)-characterized emissions in the visible range. Similarly, nonlinear curve fitting was done to unravel the solution coordination species. As depicted in Fig. 3f, the intensity changes at 545 nm, as a function of M/L ratios, could be best fitted as three-phase exponential growth process, indicating a more sophisticated coordination process for **Phen-2DIBA-re** in comparison with **Phen-2DIBA**, which probably arose from the weaker binding affinity of **Phen-2DIBA-re**.[24,57] Detailed identification of the coordination species under current conditions went outside the scope of the current manuscript. Finally, the limits of detection (LOD) for **Phen-2DIBA** and **Phen-2DIBA-re** were determined to be 15 nM and 2.95 μM, respectively (detailed calculations of LODs are given in ESI,† and Fig. S19 and S20), which were comparable to the ultra-sensitive lanthanide selective protein lanmodulin (18 nM for Tb(III)),[37] and among the highest sensing performance in aqueous conditions.[20,41]

Sensing mechanisms

To get a glimpse of the superior sensing selectivity of the current reported ligands, the coordination modes were investigated for **Phen-2DIBA** and **Phen-2DIBA-re**. The infrared spectra for the two ligands and corresponding metal complexes were compared, and the results are depicted in Fig. 4a. For **Phen-2DIBA** and **Phen-2DIBA-re**, the coordination of metal cations resulted mainly in the shifting of C=O (carbonyl groups) and C=N (phenanthroline) stretching peaks, confirming the ONNO binding nature for **Phen-2DIBA** and **Phen-2DIBA-re**.[47,48,52,58] From previous discussions, one could expect smaller Lns(III) binding constants for **Phen-2DIBA-re** with respect to **Phen-2DIBA** even though the attempt to calculate the binding

constant for **Phen-2DIBA-re** failed because of the limited solubility in single-component aqueous media (Fig. S5 and associated solubility discussions, ESI†). The highly selective sensing of Tb(III) for **Phen-2DIBA-re** indicated the existence of efficient sensitization. Furthermore, the critical role of aggregate formation for the efficient sensing by **Phen-2DIBA-re** of Tb(III) strongly indicated the importance of energy level alignment for sensitivity. Under such circumstances, the electrochemical properties of **Phen-2DIBA** and **Phen-2DIBA-re** were examined, and the results are illustrated in Fig. 4b. The energy levels for the two ligands were demonstrated through cyclic voltammetry (CV, grey lines) and differential pulse voltammetry (DPV, black lines). The reversing of imide bonds resulted in higher oxidation potential for **Phen-2DIBA-re**. Together with the red-shifted emission spectra, higher singlet and triplet energy levels could be expected for **Phen-2DIBA-re** in comparison to **Phen-2DIBA**. As demonstrated in Fig. 4c, the selectivity of **Phen-2DIBA** and **Phen-2DIBA-re** towards Eu(III) and Tb(III) could be better understood from energy level aspects, considering relative energy level alignments for aqueous Eu(III) and Tb(III) cations. Moreover, the relatively higher sensitivity of aggregated **Phen-2DIBA-re** could be rationalized as the more-favourable triplet energy levels of **Phen-2DIBA-re** aggregating to sensitize $^5D_4$ of Tb(III) cations (Fig. S21 shows the importance of **Phen-2DIBA-re** aggregates for sensitization of Tb(III) cations, ESI†). Overall,
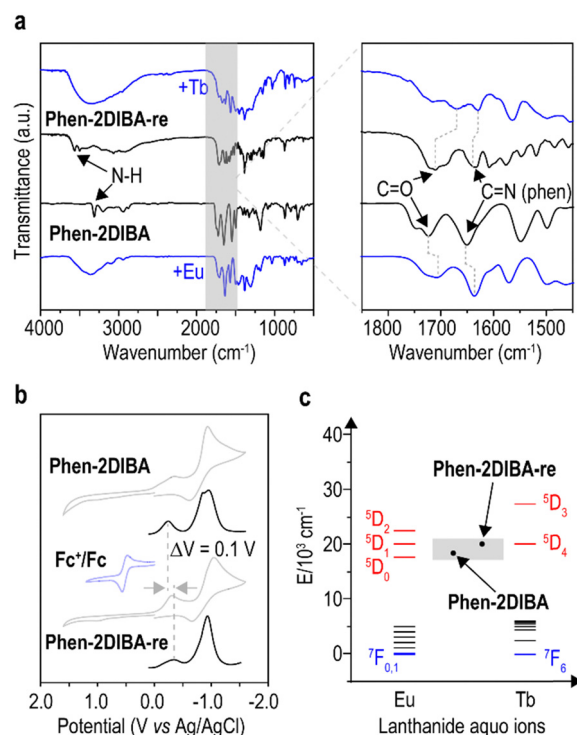

Fig. 4 Coordination modes and sensing mechanism. (a) IR spectra of **Phen-2DIBA** and **Phen-2DIBA-re** comparing corresponding metal complexes. (b) Cyclic voltammetry (CV, grey lines) and differential pulse voltammetry (DPV, black lines) of both the ligands *versus* Ag/AgCl in dry DMF. Conditions: 1 mM ligands with 100 mM NBu₄PF₆ as supporting electrolyte. (c) Illustration of the sensing mechanism for **Phen-2DIBA** and **Phen-2DIBA-re** towards Eu(III) and Tb(III).

This journal is © The Royal Society of Chemistry 2024

J. Mater. Chem. C, 2024, **12**, 6056–6063 | **6061**

the reported ligands could be more energetically selective to sensitize Eu(III) and Tb(III) in aqueous solutions and designing binding-based selective ligands, for which the ligand design principle could be readily transferred to the selective extraction, is more favoured and now underway in our group.

Conclusions

In the present study, two isomeric phenanthroline diimides and their selective Lns(III) sensing performance in aqueous solutions were demonstrated. By changing the bond sequences of phenanthroline diimide ligands while keeping same coordination environments, the structural isomerides **Phen-2DIBA** and **Phen-2DIBA-re** were straightforwardly prepared under mild reaction conditions. Close examination of the photophysical properties and density functional theory (DFT) calculations revealed that subtle structural changes induced a shift in the nature of emissive transitions, from π–π for **Phen-2DIBA** to ILCT mixed π–π for **Phen-2DIBA-re**. Notably, lanthanide-sensing experiments illustrated the highly selective sensing of Eu(III) and Tb(III) for **Phen-2DIBA** and **Phen-2DIBA-re** with superior anti-interference from other lanthanide(III) cations. Remarkably, **Phen-2DIBA** was found to be efficient towards Eu(III) even under dilute acid conditions. Meanwhile, the sensing performance of **Phen-2DIBA-re** was related to molecular aggerate formation, which could alter the energy level alignments and thus affect the sensitization of metal cations. The LODs for **Phen-2DIBA** and **Phen-2DIBA-re** were found to be 15 nM and 2.95 μM, respectively. To the best of our knowledge, this work represents a pioneering effort in unveiling lanthanide selectivity in aqueous media on the basis of molecular structure, which thus could potentially contribute to establishing the structure–function relationship for intragroup lanthanide discrimination and extraction.

Author contributions

Y. Kang, H. Li, M. Bao, Y. Zheng, L. Wang, D. Liu, J. Li, Z. Wei, C. Weng: data collection, investigation and validation. G. Wang: DFT calculation. X. Tang and L. Wang: supervision and data analysis. X. Tang and L. Wang: conceptualization, funding acquisition, project administration. X. Tang and L. Wang: writing the original draft and review & editing. All authors have given their approval to the final version of the manuscript.

Conflicts of interest

There are no conflicts to declare.

Acknowledgements

Notes and references

1 L. D. Carlos, R. A. S. Ferreira, V. D. Z. Bermudez and S. J. L. Ribeiro, *Adv. Mater.*, 2009, **21**, 509–534.

2 J.-C. G. Bünzli, *Coord. Chem. Rev.*, 2015, **293–294**, 19–47.

3 B. Zheng, J. Fan, B. Chen, X. Qin, J. Wang, F. Wang, R. Deng and X. Liu, *Chem. Rev.*, 2022, **122**, 5519–5603.

4 J.-C. G. Bünzli and C. Piguet, *Chem. Soc. Rev.*, 2005, **34**, 1048–1077.

5 Z. Liu, W. He and Z. Guo, *Chem. Soc. Rev.*, 2013, **42**, 1568–1600.

6 M. Shibasaki and N. Yoshikawa, *Chem. Rev.*, 2002, **102**, 2187–2210.

7 F. T. Edelmann, *Chem. Soc. Rev.*, 2009, **38**, 2253–2268.

8 J.-C. G. Bünzli, *J. Coord. Chem.*, 2014, **67**, 3706–3733.

9 X.-Z. Li, C.-B. Tian and Q.-F. Sun, *Chem. Rev.*, 2022, **122**, 6374–6458.

10 A. S. Weber, A. M. Grady and R. T. Koodali, *Catal. Sci. Technol.*, 2012, **2**, 683–693.

11 P. S. Arshi, E. Vahidi and F. Zhao, *ACS Sustainable Chem. Eng.*, 2018, **6**, 3311–3320.

12 J.-C. G. Bünzli, *Chem. Rev.*, 2010, **110**, 2729–2755.

13 T. I. Kostelnik and C. Orvig, *Chem. Rev.*, 2019, **119**, 902–956.

14 Y. Ning, M. Zhu and J.-L. Zhang, *Coord. Chem. Rev.*, 2019, **399**, 213028.

15 D. S. Sholl and R. P. Lively, *Nature*, 2016, **532**, 435–437.

16 T. Cheisson and E. J. Schelter, *Science*, 2019, **363**, 489–493.

17 Y. Geng, J. Sarkis and R. Bleischwitz, *Nature*, 2023, **619**, 248–251.

18 V. Gonzalez, D. A. L. Vignati, C. Leyval and L. Giamberini, *Environ. Int.*, 2014, **71**, 148–157.

19 V. Balaram, *Geosci. Front.*, 2019, **10**, 1285–1303.

20 S. E. Crawford, P. R. Ohodnicki and J. P. Baltrus, *J. Mater. Chem. C*, 2020, **8**, 7975–8006.

21 Y. Fang and W. Dehaen, *Coord. Chem. Rev.*, 2021, **427**, 213524.

22 M. D. Ward, *Coord. Chem. Rev.*, 2010, **254**, 2634–2642.

23 M. R. Ganjali, B. Veismohammadi, M. Hosseini and P. Norouzi, *Spectrochim. Acta, Part A*, 2009, **74**, 575–578.

24 P. Das, A. Ghosh and A. Das, *Inorg. Chem.*, 2010, **49**, 6909–6916.

25 M. R. Ganjali, V. K. Gupta, M. Hosseini, M. Hariri, F. Faridbod and P. Norouzi, *Sens. Actuators, B*, 2012, **171–172**, 644–651.

26 M. R. Ganjali, M. Hosseini, A. Ghafarloo, M. Khoobi, F. Faridbod, A. Shafiee and P. Norouzi, *Mater. Sci. Eng., C*, 2013, **33**, 4140–4143.

27 L. Huang, Y. Liu, C. Ma, P. Xi, W. Kou and Z. Zeng, *Dyes Pigm.*, 2013, **96**, 770–773.

28 S. Areti, S. Bandaru, R. Teotia and C. P. Rao, *Anal. Chem.*, 2015, **87**, 12348–12354.

29 F. Faridbod, M. Sedaghat, M. Hosseini, M. R. Ganjali, M. Khoobi, A. Shafiee and P. Norouzi, *Spectrochim. Acta, Part A*, 2015, **137**, 1231–1234.

30 Q. Zhao, X.-M. Liu, H.-R. Li, Y.-H. Zhang and X.-H. Bu, *Dalton Trans.*, 2016, **45**, 10836–10841.

31 Y.-H. Huang, Q.-X. Geng, X.-Y. Jin, H. Cong, F. Qiu, L. Xu, Z. Tao and G. Wei, *Sens. Actuators, B*, 2017, **243**, 1102–1108.

32 H. Zhang, T. Liu, C. Yin, Y. Wen, J. Chao, Y. Zhang and F. Huo, *Spectrochim. Acta, Part A*, 2017, **174**, 230–235.

33 Q. Chen, J. Zuo, X. He, X. Mo, P. Tong and L. Zhang, *Talanta*, 2017, **162**, 540–546.

34 S. Wang, S. Liu, J. Zhang and Y. Cao, *Talanta*, 2019, **198**, 501–509.

35 M. Li, G. Ren, F. Wang, Z. Li, W. Yang, D. Gu, Y. Wang, G. Zhu and Q. Pan, *Inorg. Chem. Front.*, 2019, **6**, 1129–1134.

36 A. Shaikh, P. Mukherjee, S. Ta, A. Bhattacharyya, A. Ghosh and D. Das, *New J. Chem.*, 2020, **44**, 9452–9455.

37 E. R. Featherston, E. J. Issertell and J. A. Cotruvo, Jr., *J. Am. Chem. Soc.*, 2021, **143**, 14287–14299.

38 X.-X. Liu, L.-P. Lu and M.-L. Zhu, *Sens. Actuators, B*, 2021, **347**, 130641.

39 L. Zang, C. Luan, X. Tang, J. Lu and Y. Zhao, *Dyes Pigm.*, 2021, **196**, 109751.

40 M.-M. Fu, L. Fu and G.-H. Cui, *Dalton Trans.*, 2021, **50**, 10180–10186.

41 D. Bhowmik and U. Maitra, *Chem. Sci.*, 2023, **14**, 4901–4904.

42 L. Duan, J. Fan, D. Tian, Y. Kang, Q. Wu, X. Zhang, P. Li, L. Wang, G. Shen and P. Qiu, *Colloids Surf., A*, 2023, **663**, 131019.

43 W.-R. Shin, G. Ahn, J.-P. Lee, I.-H. Oh, J.-Y. Ahn, Y.-H. Kim and S. Chae, *Chem. Eng. J.*, 2023, **472**, 144742.

44 L. Xu, X. Yang, A. Zhang, C. Xu and C. Xiao, *Coord. Chem. Rev.*, 2023, **496**, 215404.

45 Y. Wang, K. M. Shield and R. J. Abergel, *Sep. Purif. Rev.*, 2023, 1–19, DOI: 10.1080/15422119.2023.2182220.

46 L. Götzke, G. Schaper, J. März, P. Kaden, N. Huittinen, T. Stumpf, K. K. K. Kammerlander, E. Brunner, P. Hahn, A. Mehnert, B. Kersting, T. Henle, L. F. Lindoy, G. Zanoni and J. J. Weigand, *Coord. Chem. Rev.*, 2019, **386**, 267–309.

47 D. Tian, Y. Liu, Y. Kang, Y. Zhao, P. Li, C. Xu and L. Wang, *ACS Cent. Sci.*, 2023, **9**, 1642–1649.

48 Y. Liu, Y. Kang, M. Bao, H. Cao, C. Weng, X. Dong, H. Hao, X. Tang, J. Chen, L. Wang and C. Xu, *J. Hazard. Mater.*, 2024, **462**, 132756.

49 Y. Liu, M. Bao, L. Wang, Y. Kang, Y. Dou, J. Qin, F. Guo, H. Hao, Z. Wang, X. Tang, J. Chen, L. Wang and C. Xu, *Chem. Eng. J.*, 2024, **485**, 149730.

50 We recent found that phenantrholine diimide ligand with hydroxyl groups would form different crystals along the lanthanides seriers, leading to the unexpected high affinity towards light lanthanides. These results would be published soon.

51 M. Yamada, K. Araki and S. Shiraishi, *Bull. Chem. Soc. Jpn.*, 1987, **60**, 3149–3155.

52 L. Duan, J. Fan, D. Tian, Q. Yan, X. Zhang, P. Li, C. Xu and L. Wang, *Colloids Surf., A*, 2022, **647**, 129089.

53 P. J. Panak and A. Geist, *Chem. Rev.*, 2013, **113**, 1199–1236.

54 K. Binnemans, *Coord. Chem. Rev.*, 2015, **295**, 1–45.

55 A. A. Essawy, *Sens. Actuators, B*, 2014, **196**, 640–646.

56 F.-Y. Yi, J.-P. Li, D. Wu and Z.-M. Sun, *Chem. – Eur. J.*, 2015, **21**, 11475–11482.

57 P. Thordarson, *Chem. Soc. Rev.*, 2011, **40**, 1305–1323.

58 P. Ren, P.-w Huang, X.-f Yang, Y. Zou, W.-q Tao, S.-l Yang, Y.-h Liu, Q.-y Wu, L.-y Yuan, Z.-f Chai and W.-q Shi, *Inorg. Chem.*, 2021, **60**, 357–365.